

Temperature dependence of Raman scattering in AlInN

L. F. Jiang,¹ J. F. Kong,² W. Z. Shen,^{1,a)} and Q. X. Guo³

¹Laboratory of Condensed Matter Spectroscopy and Opto-Electronic Physics, Key Laboratory of Artificial Structures and Quantum Control (Minister of Education), Department of Physics, Shanghai Jiao Tong University, 800 Dong Chuan Road, Shanghai 200240, People's Republic of China

²Department of Physics, Shanghai Institute of Technology, 100 Hai Quan Road, Shanghai 201418, People's Republic of China

³Synchrotron Light Application Center, Department of Electrical and Electronic Engineering, Saga University, Saga 840-8502, Japan

(Received 28 January 2011; accepted 22 April 2011; published online 6 June 2011)

A detailed investigation of temperature-dependent micro-Raman scattering has been carried out on AlInN films with different Al compositions (0–0.53). The observed phonon frequency downshift and linewidth broadening with increasing temperature can be well explained by a model taking into account the contributions of the thermal expansion, the lattice-mismatch-induced strain, and the anharmonic phonon processes. It is found that with increasing Al composition the three-phonon process increases over the four-phonon process, but still is not the obvious prevailing process in the phonon decay of AlInN. We have attributed it to the variation of structural properties and phonon density of states in AlInN. © 2011 American Institute of Physics. [doi:10.1063/1.3594697]

I. INTRODUCTION

As a wide variable bandgap semiconductor, ternary AlInN has great potential for applications in light-emitting diodes, laser diodes, solar cells, high-electron-mobility transistors, and highly reflective distributed Bragg reflectors in the ultraviolet region.^{1–10} For example, Al_{0.83}In_{0.17}N has been used as a strain free cladding layer on a GaN-based laser diode structure, leading to a reduction in the number of defects because it is lattice-matched to GaN.^{3–5} In order to fulfill AlInN applications in commercially optical and electronic devices, the fundamental properties of this material have been studied experimentally^{1–11} and theoretically.^{12–14} Starosta¹¹ has reported the first synthesis of AlInN polycrystalline films by a reactive multitarget sputtering method. Subsequently, there have been numerous reports about the growth of single phase AlInN by a variety of methods,^{1,3,5,7} with the emphasis on improving the quality, due to the large differences in chemical and physical parameters between InN and AlN. Another crucial step toward the realization of AlInN-based devices is to clearly understand the structural and optical properties. X-ray diffraction,^{1,2} photoluminescence,^{3,4,8} transmission,^{2,8} and reflection^{5–7} spectroscopies have been carried out for Al-related characteristics of emission and bandgap engineering in AlInN.

In comparison with other spectroscopic techniques, Raman scattering possesses the advantages of nondestructive, contactless, and no special sample preparation such as thinning or polishing. Therefore, Raman spectroscopy has been widely employed in AlInN at room temperature.^{5,9,10,14} However, in contrast to the comprehensive investigation of temperature effect of Raman scattering for the binary nitride semiconductors of InN^{15,16} and AlN,^{17–19} there is no detailed temperature dependence of phonon behavior in AlInN.

Extensive investigation has been carried out in InN and AlN, indicating that three-phonon process is almost the same as the four-phonon process in the decay of A₁[longitudinal optical (LO)] in InN,¹⁵ while the three-phonon process is the prevailing process in the decay of A₁(LO) and E₂(high) in AlN.¹⁷ The introduction of Al in InN is substituted with In atom, where the random distribution leads to fluctuations of the force constants in the neighborhood, and therefore results in compositional disorder. This brings on a violation of the translational symmetry. What is the phonon decay characteristics in AlInN and how the decay process is related with the Al composition are still open questions.

In this paper, we have presented a comprehensive micro-Raman investigation of temperature-dependent phonon properties of A₁(LO), A₂(LO), and E₂(high) modes in AlInN films with different Al compositions (0–0.53) in the temperature range from 83 to 473 K. In combination with a detailed theoretical modeling for the frequency downshift and linewidth broadening, we have clearly illustrated the temperature effect on the phonon frequencies and linewidths in the ternary AlInN thin films.

II. EXPERIMENTAL DETAILS

The studied AlInN films were grown on (0001) sapphire substrates by reactive rf magnetron sputtering in an ambient of argon and nitrogen.⁷ The sapphire substrate temperature was monitored using a thermocouple and controlled at 100 °C. During the growth, the total gas flow rate and pressure were maintained at 8 sccm and 2 mTorr, respectively. The indium and aluminum plates were separately mounted onto the targets and were simultaneously sputtered at different rf powers, while the substrate holder was rotated at a constant rate of 36 rpm. The Al composition was measured by energy-dispersive x-ray spectroscopy. Five Al_xIn_{1–x}N samples with the Al composition *x* of 0, 0.26, 0.38, 0.46, and 0.53 were selected in the present study. Temperature-

^{a)}Author to whom correspondence should be addressed. Electronic mail: wzshen@sjtu.edu.cn.

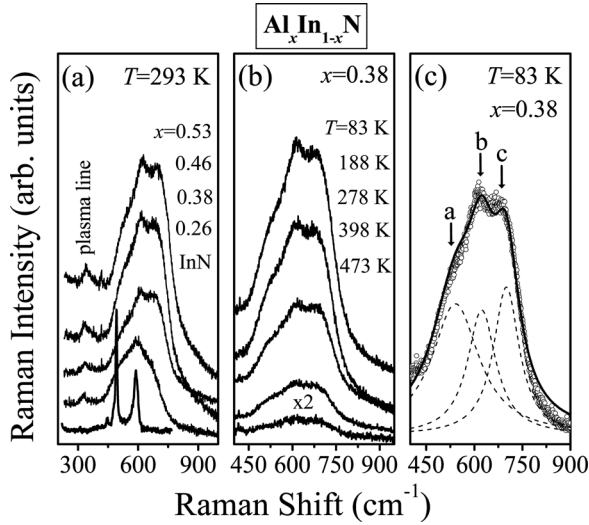


FIG. 1. (a) Raman spectra of AlInN with different Al compositions at 293 K. (b) Temperature-dependent Raman spectra of $\text{Al}_{0.38}\text{In}_{0.62}\text{N}$. (c) Raman spectrum of $\text{Al}_{0.38}\text{In}_{0.62}\text{N}$ at 83 K, where the solid curve is the fitting results using three Lorentz peaks (dashed curves) with a: $E_2(\text{high})$, b: $A_1(\text{LO})$, and c: $A_2(\text{LO})$.

dependent micro-Raman scattering spectra from 83 to 473 K were recorded in a backscattering geometry of $z(x, -)\bar{z}$ configuration using a Jobin Yvon LabRAM HR 800UV system under the 514.5 nm line of an Ar-ion laser. The employment of a $50\times$ optical microscopy objective with a numerical aperture of 0.5 will yield a laser spot size of $\sim 1.3\ \mu\text{m}$.

III. RESULTS AND DISCUSSION

Figure 1(a) shows the first-order micro-Raman spectra of AlInN films with different Al compositions at 293 K. The sharp Raman peaks of InN located at 495 and $597\ \text{cm}^{-1}$ correspond to $E_2(\text{high})$ and $A_1(\text{LO})$ phonon modes,¹⁵ respectively, while the $\sim 340\ \text{cm}^{-1}$ is attributed to the plasma line.⁵ It is clear that the peaks become broadened and some other Raman structures show up, with the Al composition increasing. Figure 1(b) presents the temperature-dependent micro-Raman spectra of $\text{Al}_{0.38}\text{In}_{0.62}\text{N}$. The peak shifts to low frequency with the increase of temperature. In order to identify each of the contributions, we have fitted the observed Raman spectra with Lorentz peaks. Figure 1(c) shows the detailed analysis of the experimental Raman spectrum (circles) for $\text{Al}_{0.38}\text{In}_{0.62}\text{N}$ at 83 K with three peaks (dashed curves) a, b, and c at about 525 , 625 , and $682\ \text{cm}^{-1}$, respectively. A correction of the measured Raman linewidths with respect to the spectral resolution of the spectrometer led to a change in the linewidth of less than 3% and could therefore be omitted.¹⁷ From the peak positions, we can assign the contribution a, b, and c to the $E_2(\text{high})$ -, $A_1(\text{LO})$ -, and $A_2(\text{LO})$ -phonon modes of AlInN, respectively.¹⁴ The above Lorentz fitting processes are employed to obtain the detailed temperature and Al-composition dependencies of the phonon frequency and linewidth. In the following, we concentrate on the phonon characteristics of the $A_1(\text{LO})$, $A_2(\text{LO})$, and $E_2(\text{high})$ modes in the $\text{Al}_x\text{In}_{1-x}\text{N}$ alloy.

Figure 2 illustrates the frequencies of the $A_1(\text{LO})$, $A_2(\text{LO})$, and $E_2(\text{high})$ modes with temperature. To demon-

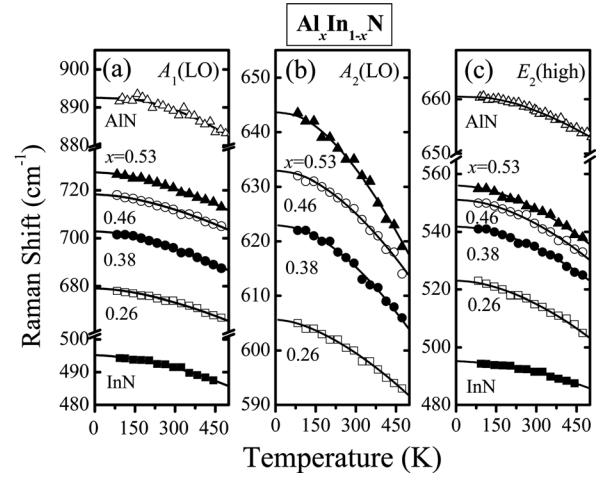


FIG. 2. Temperature-dependent Raman frequencies of (a) $A_1(\text{LO})$, (b) $A_2(\text{LO})$, and (c) $E_2(\text{high})$ modes in AlInN with different Al compositions. The solid curves are the theoretical calculation results with Eqs. (1) and (2). Also shown for comparison are the experimental results of AlN from Ref. 17.

strate the reliability of the obtained modes, we have also shown the experimental results of AlN from Ref. 17 in Figs. 2(a) and 2(c). The downshift of the phonon frequency with the increase of temperature can be described by the perturbation model which the frequency shift is mainly due to the effects of the thermal expansion, the lattice-mismatch-induced strain, and the anharmonic coupling to other phonons.¹⁵ The Raman frequency can be expressed as a function of temperature as:

$$\omega(T) = \omega_0 + \Delta\omega_e(T) + \Delta\omega_s(T) + \Delta\omega_d(T) \quad (1)$$

with ω_0 the harmonic frequency of the optical mode, $\Delta\omega_e(T)$ the contribution of thermal expansion or volume change, $\Delta\omega_s(T)$ the lattice and thermal mismatch between the AlInN thin film and sapphire substrate, and $\Delta\omega_d(T)$ the one due to the anharmonic coupling to phonons of other branches. The term $\Delta\omega_e(T)$ can be written as $\Delta\omega_e(T) = -\omega_0\gamma \int_0^T [\alpha_c(T') + 2\alpha_a(T')]dT'$, where γ is the mode Grüneisen parameter,^{15,20} α_c and α_a are the temperature-dependent linear thermal expansion coefficients parallel and perpendicular to the c axis, respectively.^{15,21} The strain-induced term $\Delta\omega_s(T)$ can be given by $\Delta\omega_s(T) = [2a - (2C_{13}/C_{33})b]\varepsilon(T)$, with $\varepsilon(T)$ the temperature dependence of in-plane strain for the different thermal expansion coefficients between thin films and substrates.^{15,21} The phonon deformation potentials a and b , as well as the elastic constants C_{13} and C_{33} , are taken from Refs. 15 and 17.

Taking into account cubic and quartic terms in the anharmonic Hamiltonian, we have the term $\Delta\omega_d(T)$ as:²²

$$\Delta\omega_d(T) = M_1[1 + n(T, \omega_1) + n(T, \omega_2)] + M_2[1 + 3n(T, \omega_0/3) + 3n^2(T, \omega_0/3)], \quad (2)$$

where $n(T, \omega) = [\exp(\hbar\omega/k_B T) - 1]^{-1}$ is the Bose-Einstein function. In Eq. (2), the first term corresponds to the decay into two phonons of frequency ω_1 and ω_2 (three-phonon process), with $\omega_1 + \omega_2 = \omega_0$; while the second term accounts

TABLE I. The best fitting parameters for Raman frequencies [Eqs. (1) and (2)] and linewidths [Eq. (3)] of the $A_1(\text{LO})$, $A_2(\text{LO})$, and $E_2(\text{high})$ modes in AlInN.

Raman modes	$\text{Al}_x\text{In}_{1-x}\text{N}$	ω_0 (cm^{-1})	M_1 (cm^{-1})	M_2 (cm^{-1})	Γ_0 (cm^{-1})	N_1 (cm^{-1})	N_2 (cm^{-1})
$A_1(\text{LO})$	0	597.6	-0.37	-0.27	15.7	0.20	0.19
	0.26	681.7	-1.60	-0.89	88.1	3.08	1.65
	0.38	705.1	-1.86	-0.95	93.5	3.79	1.80
	0.46	723.7	-2.39	-1.07	95.3	4.64	1.91
	0.53	728.9	-2.87	-1.13	97.2	5.10	1.94
$A_2(\text{LO})$	0.26	608.1	-1.58	-0.73	93.3	3.82	1.55
	0.38	625.0	-2.02	-0.92	100.2	4.22	1.65
	0.46	639.7	-2.36	-0.98	121.5	5.62	2.08
	0.53	645.8	-2.71	-1.02	124.1	6.60	2.30
$E_2(\text{high})$	0	494.9	0	-0.39	5.7	0	0.70
	0.26	525.3	-1.14	-1.10	136.3	5.01	4.74
	0.38	545.8	-1.32	-1.14	155.2	8.98	7.68
	0.46	554.3	-1.81	-1.31	160.8	14.20	9.80
	0.53	562.0	-2.12	-1.33	172.1	22.30	14.10

for the decay into three phonons (four-phonon process), considering simply equal frequency $\omega_0/3$. We have employed the linear dependence of the Al content for the values of ω_1 and ω_2 in AlInN. M_1 and M_2 are anharmonic constants which are related to the relative probability of the occurrence of each process. Generally, the simplest three-phonon process for optical phonon decay, proposed by Klemens, is the decay into acoustic phonons of equal energy, $\omega_1 = \omega_2$, and opposite.²³ However, in the case of InN, the zone-center LO phonons cannot decay into two longitudinal acoustic (LA) or transverse acoustic (TA) phonons of equal frequency and opposite wave vector in the three-phonon process due to the large energy gap between the acoustic and optical phonon branches in InN ($2\omega_{\text{LA,TA}} < \omega_{\text{LO}}$). The possibility is to decay into a large wave-vector transverse optical (TO) phonon and a large wave-vector TA phonon.¹⁶ On the other hand, since the energy gap between the acoustic- and the optical-phonon branches is more than one half of the $E_2(\text{high})$ phonon energy, the $E_2(\text{high})$ phonon of InN cannot decay into either two LA (TA) phonons or one TO and one LA (TA) phonons [$E_2(\text{high})$ is at the lower edge of the optical-phonon branch].¹⁵ As a result, only the four-phonon process has been taken into account in the decay of the $E_2(\text{high})$ phonon in InN. Therefore, we have employed the similar decay processes for the temperature dependence of Raman frequencies of $A_1(\text{LO})$, $A_2(\text{LO})$, and $E_2(\text{high})$ in AlInN films, and have found good agreement with the experimental data shown in Fig. 2.

The solid curves in Fig. 2 are the calculated $A_1(\text{LO})$, $A_2(\text{LO})$, and $E_2(\text{high})$ phonon frequencies with temperatures using Eqs. (1) and (2) with ω_0 , M_1 , and M_2 as fitting parameters (listed in Table I). The other parameters for AlInN are obtained by linear interpolation method from those of InN and AlN. The Raman frequency of the three modes in AlInN is found to increase linearly with Al composition, which has also been observed by Kang *et al.*¹⁴ In addition to a blueshift in the Raman frequency of AlInN compared with that of InN,^{15,16} we note that the variation of ω_0 with Al composition can be attributed well to the change of the lattice constant. Due to the incorporation of Al substitutionally on the In sublattice, the lattice constant decreases with the increase

of Al composition,^{9,24} resulting in the increase of ω_0 . Furthermore, we can also clearly observe that the anharmonic constants M_1 and M_2 of the three modes in AlInN are higher than those in pure InN. In AlInN, the alloy-induced disorder brings on an increase of phonon density of states (DOS) which leads to the enhancement of the probability of inelastic (anharmonic) scattering between the phonons and substitutional atoms. Therefore, the contribution from anharmonicity due to the alloy-induced disorder prevails with increasing Al composition. On the other hand, larger numbers of phonons are produced with increasing temperature, which also enhances the probability of inelastic (anharmonic) scattering between the phonons and substitutive atoms. As a result, the alloy-disorder anharmonicity becomes more obvious with the increase of temperature in AlInN.

The phonon broadening $\Gamma(T)$ mainly comes from inhomogeneous impurity phonon scattering and anharmonic decay. Similar to the temperature dependence of Raman shift, the phonon broadening can be described by assuming the decay into two phonons with frequency ω_1 and ω_2 and the symmetric decay into three phonons again:¹⁵

$$\Gamma(T) = \Gamma_0 + N_1[1 + n(T, \omega_1) + n(T, \omega_2)] + N_2[1 + 3n(T, \omega_0/3) + 3n^2(T, \omega_0/3)], \quad (3)$$

where Γ_0 denotes a damping contribution due to inherent defect or impurity scattering. The second term displays the asymmetric decay of three-phonon process, while the third term is the corresponding symmetric decay of four-phonon process. Anharmonic constants of N_1 and N_2 are the relative probability of the decay into either two or three phonons, respectively. Figure 3 shows the least-squares fit of Eq. (3) (solid curves) for the temperature-dependent linewidths of the $A_1(\text{LO})$, $A_2(\text{LO})$, and $E_2(\text{high})$ modes in AlInN. The fitting parameters Γ_0 , N_1 , and N_2 have also been given in Table I. Also shown in Figs. 3(a) and 3(c) are the experimental results of AlN from Ref. 17. It can be clearly seen that there is a rapid increase in Γ_0 between AlInN and InN due to the formation of lattice defect and structural disorder after Al incorporation. In fact, the dependence of Γ_0 on the Al composition does display the closely related behavior with that

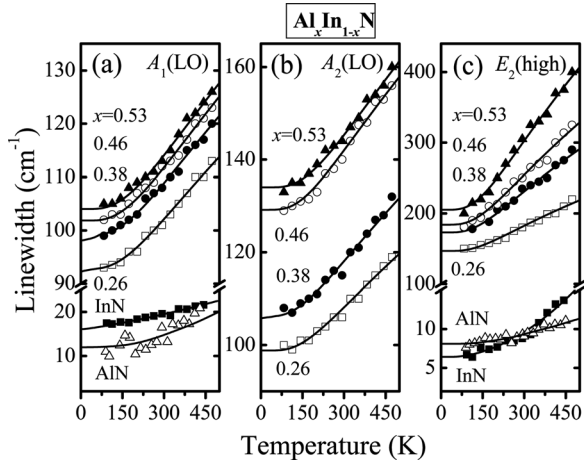


FIG. 3. Temperature-dependent Raman linewidths of (a) $A_1(\text{LO})$, (b) $A_2(\text{LO})$, and (c) $E_2(\text{high})$ modes in AlInN with different Al compositions. The solid curves are the theoretical calculation results with Eq. (3). Also shown for comparison are the experimental results of AlN from Ref. 17.

of Urbach band tail in Ref. 8. On the other hand, the linewidth of $E_2(\text{high})$ mode is found to be smaller than that of $A_1(\text{LO})$ phonon in InN , because the $E_2(\text{high})$ phonon of InN can only decay into three phonons. However, the linewidth of $E_2(\text{high})$ phonon increases much more rapidly with Al composition than that of $A_1(\text{LO})$ phonon, which has also been found by Butte *et al.*,⁵ and Naik *et al.*¹⁰ This possibly indicates that there are more channels for the decay of the $E_2(\text{high})$ mode than for the decay of the $A_1(\text{LO})$ phonon in AlInN .

From the ratios of M_1/M_2 and N_1/N_2 , the relative contributions of the three-phonon and four-phonon processes to the total phonon decay can be estimated. Figure 4 presents the ratios of M_1/M_2 and N_1/N_2 for the $A_1(\text{LO})$, $A_2(\text{LO})$, and $E_2(\text{high})$ modes of AlInN , respectively. For InN , the ratios of M_1/M_2 and N_1/N_2 for the $A_1(\text{LO})$ mode are very close to 1.0, indicating that the probability of the three-phonon process is almost the same as the four-phonon one in the anharmonic coupling of the $A_1(\text{LO})$ mode. In contrast, the ratios of M_1/M_2 and N_1/N_2 for the $E_2(\text{high})$ mode of InN are zero, since the $E_2(\text{high})$ phonon of InN can only decay into three phonons.¹⁵ With increasing Al composition, the ratios of M_1/M_2 and N_1/N_2 increase for all the three modes in AlInN , revealing the increasing contribution of the three-phonon process over the four-phonon one. However, the ratios in AlInN are much less than those in AlN [M_1/M_2 (N_1/N_2) ~ 10 and ~ 50 for the $A_1(\text{LO})$ and $E_2(\text{high})$ modes, respectively],¹⁷ demonstrating that the three-phonon process is not the obvious prevailing process in the phonon decay of ternary AlInN . The consistent variation between M_1/M_2 and N_1/N_2 with Al composition in these three phonon modes further indicates the reliability of our results obtained from the theoretical fitting. Moreover, according to our calculation, the ratios of M_1/M_2 and N_1/N_2 will be changed $\sim 1\%$, if there is 5% systematic error in $\Delta\omega_e(T)$ as a function of Al content. However, a systematic error in $\Delta\omega_s(T)$ is almost no effect on M_1/M_2 and N_1/N_2 .

We attribute the change of M_1/M_2 and N_1/N_2 to the fluctuation in phonon DOS due to the increase of ω_0 with Al

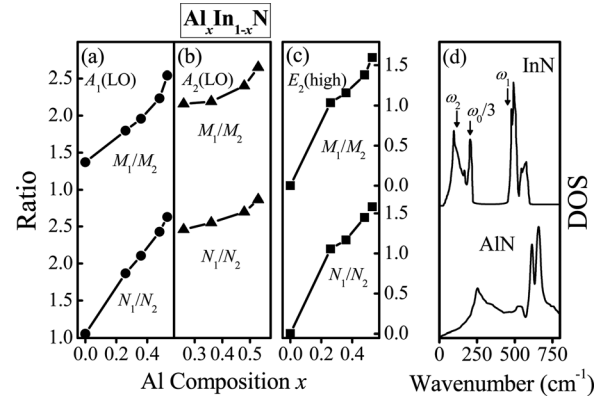


FIG. 4. Al-composition dependence of ratios M_1/M_2 and N_1/N_2 for (a) $A_1(\text{LO})$, (b) $A_2(\text{LO})$, and (c) $E_2(\text{high})$ modes in AlInN . (d) Calculated phonon DOS of InN (from Ref. 25) and AlN (from Ref. 26), with the positions of ω_1 (TO phonon in InN), ω_2 (TA phonon in InN), and $\omega_0/3$ marked.

composition. The incorporation of Al in InN causes lattice defect and structural disorder, which break down the translational symmetry of InN . As a consequence, not only the Brillouin zone-center phonons but also the phonons at Brillouin zone-edges have contribution to the first-order Raman scattering. From the phonon DOS of InN (Ref. 25) and AlN (Ref. 26) shown in Fig. 4(d), on one hand, the increase of ω_0 with Al composition leads to a decrease of the phonon DOS in AlInN at $\omega_0/3$ ($\sim 190 \text{ cm}^{-1}$) due to the significant decrease of InN phonon DOS there [see arrow in Fig. 4(d)], i.e., the reduction of the four-phonon process contribution. On the other hand, the increase of ω_0 in AlInN causes large values of ω_1 and ω_2 . Considering $\omega_1 \sim 480 \text{ cm}^{-1}$ and $\omega_2 \sim 117 \text{ cm}^{-1}$, the blueshift of ω_1 and ω_2 in AlInN results in an increase of phonon DOS [see arrows in Fig. 4(d)], which brings on the increase of the contribution of the three-phonon process. Therefore, as shown in Figs. 4(a)–4(c), the values of M_1/M_2 and N_1/N_2 in AlInN are larger than those of InN , and the dependences of M_1/M_2 and N_1/N_2 on Al composition, as expected, have the similar variation law to ω_0 listed in Table I. The above results demonstrate unambiguously that with the increase of Al composition in AlInN the three-phonon process gradually enhances the anharmonic shift and broadening of the $A_1(\text{LO})$, $A_2(\text{LO})$, and $E_2(\text{high})$ modes, though the four-phonon process is adequately responsible for the anharmonic decay process.

IV. CONCLUSIONS

In summary, we have investigated in detail the temperature-dependent micro-Raman scattering of $\text{Al}_x\text{In}_{1-x}\text{N}$ ($0 \leq x \leq 0.53$) thin films grown by reactive rf magnetron sputtering on sapphire substrates under the temperature range of 83–473 K. The temperature-dependent phonon frequencies and linewidths of the $A_1(\text{LO})$, $A_2(\text{LO})$, and $E_2(\text{high})$ modes in AlInN have been obtained through Lorentz fitting. By the aid of a model involving the contributions of the thermal expansion, lattice-mismatch-induced strain, as well as three- and four-phonon coupling, we have clearly illustrated the temperature effect on the phonon frequency and linewidth of AlInN . We have demonstrated that with increasing

Al composition the contribution of the three-phonon process increases while that of four-phonon process reduces, due to the variation of structural properties and phonon DOS in AlInN. The phonon properties provide an experimental basis for further theoretical investigation and the design of AlInN-based devices.

ACKNOWLEDGMENTS

This work was supported by the National Major Basic Research Project of 2010CB933702 and the Natural Science Foundation of China under contract 10734020.

- ¹Q. X. Guo, T. Tanaka, M. Nishio, and H. Ogawa, *Jpn. J. Appl. Phys.* **42**, L141 (2003).
- ²R. E. Jones, R. Broesler, K. M. Yu, J. W. Ager, E. E. Haller, W. Walukiewicz, X. Chen, and W. J. Schaff, *J. Appl. Phys.* **104**, 123501 (2008).
- ³K. Wang, R. W. Martin, D. Amabile, P. R. Edwards, S. Hernandez, E. Nogales, K. P. O'Donnell, K. Lorenz, E. Alves, V. Matias, A. Vantomme, D. Wolfverson, and I. M. Watson, *J. Appl. Phys.* **103**, 073510 (2008).
- ⁴S. Yamaguchi, M. Kariya, S. Nitta, T. Takeuchi, C. Wetzel, H. Amano, and I. Akasaki, *Appl. Phys. Lett.* **76**, 876 (2000).
- ⁵R. Butte, J.-F. Carlin, E. Feltn, M. Gonschorek, S. Nicolay, G. Christmann, D. Simeonov, A. Castiglia, J. Dorsaz, H. J. Buehlmann, S. Christopoulos, G. B. H. von Hogerthal, A. J. D. Grundy, M. Mosca, C. Piquier, M. A. Py, F. Demangeot, J. Frandon, P. G. Lagoudakis, J. J. Baumberg, and N. Grandjean, *J. Phys. D: Appl. Phys.* **40**, 6328 (2007).
- ⁶J.-F. Carlin and M. Illegems, *Appl. Phys. Lett.* **83**, 668 (2003).
- ⁷Q. X. Guo, T. Tanaka, M. Nishio, and H. Ogawa, *Jpn. J. Appl. Phys.* **47**, 612 (2008).
- ⁸L. F. Jiang, W. Z. Shen, and Q. X. Guo, *J. Appl. Phys.* **106**, 013515 (2009).
- ⁹V. Darakchieva, M.-Y. Xie, F. Tasnádi, I. A. Abrikosov, L. Hultman, B. Monemar, J. Kamimura, and K. Kishino, *Appl. Phys. Lett.* **93**, 261908 (2008).
- ¹⁰V. M. Naik, W. H. Weber, D. Uy, D. Haddad, R. Naik, Y. V. Danylyuk, M. J. Lukitsch, G. W. Auner, and L. Rimai, *Appl. Phys. Lett.* **79**, 2019 (2001).
- ¹¹K. Starosta, *Phys. Status Solidi A* **68**, K55 (1981).
- ¹²A. F. Wright and J. S. Nelson, *Appl. Phys. Lett.* **66**, 3465 (1995).
- ¹³H. Grille, Ch. Schnittler, and F. Bechstedt, *Phys. Rev. B* **61**, 6091 (2000).
- ¹⁴T. T. Kang, A. Hashimoto, and A. Yamamoto, *Phys. Rev. B* **79**, 033301 (2009).
- ¹⁵X. D. Pu, J. Chen, W. Z. Shen, H. Ogawa, and Q. X. Guo, *J. Appl. Phys.* **98**, 033527 (2005).
- ¹⁶J. W. Pomeroy, M. Kuball, H. Lu, W. J. Schaff, X. Wang, and A. Yoshikawa, *Appl. Phys. Lett.* **86**, 223501 (2005).
- ¹⁷A. Link, K. Bitzer, W. Limmer, R. Sauer, C. Kirchner, V. Schwegler, M. Kamp, D. G. Ebling, and K. W. Benz, *J. Appl. Phys.* **86**, 6256 (1999).
- ¹⁸M. Kuball, J. M. Hayes, Y. Shi, and J. H. Edgar, *Appl. Phys. Lett.* **77**, 1958 (2000).
- ¹⁹J. M. Hayes, M. Kuball, Y. Shi, and J. H. Edgar, *Jpn. J. Appl. Phys.* **39**, L710 (2000).
- ²⁰M. Kuball, J. M. Hayes, A. D. Prines, N. W. A. van Uden, D. J. Dunstan, Y. Shi, and J. H. Edgar, *Appl. Phys. Lett.* **78**, 724 (2001).
- ²¹H. Iwanaga, A. Kunishige, and S. Takeuchi, *J. Mater. Sci.* **35**, 2451 (2000).
- ²²J. Jiménez, E. Martín, A. Torres, and J. P. Landesman, *Phys. Rev. B* **58**, 10463 (1998).
- ²³P. G. Klemens, *Phys. Rev.* **148**, 845 (1966).
- ²⁴B. T. Liou, Y. S. Yen, and Y. K. Kuo, *Appl. Phys. A* **81**, 651 (2005).
- ²⁵V. Yu. Davydov, V. V. Emtsev, I. N. Goncharuk, A. N. Smirnov, V. D. Petrikov, V. V. Mamutin, V. A. Vekshin, S. V. Ivanov, M. B. Smirnov, and T. Inushima, *Appl. Phys. Lett.* **75**, 3297 (1999).
- ²⁶V. Yu. Davydov, Yu. E. Kitaev, I. N. Goncharuk, A. N. Smirnov, J. Graul, O. Semchinova, D. Uffmann, M. B. Smirnov, A. P. Mirgorodsky, and R. A. Evarestov, *Phys. Rev. B* **79**, 12899 (1998).